AIAA JOURNAL
Vol. 34, No. 2, February 1996

Analysis of Cracked Aluminum Plates Repaired with Bonded Composite Patches

C. T. Sun,* J. Klug,† and C. Arendt‡
Purdue University, West Lafayette, Indiana 47907-1282

Bonded composite repair has been recognized as an efficient and economical method to extend the service life of cracked aluminum components. An accurate tool for investigating the stress intensity factor in the cracked aluminum structure after repair is needed. The use of three-dimensional finite elements is computationally expensive. A simple analysis method using Mindlin plate theory is presented. Specifically, the aluminum plate and composite patch are modeled separately by the Mindlin plate finite element, whereas the adhesive layer is modeled with effective springs connecting the patch and aluminum plate. Constraint equations are used to enforce compatibility of the patch-adhesive and adhesive-aluminum plate interfaces. Comparison of the present stress intensity factors for the aluminum crack with a plane boundary element analysis and a three-dimensional finite element analysis are made. A procedure for calculating the strain energy release rate along the debond front at the aluminum-adhesive interface is proposed.

Nomenclature

a^*, b^*	= debond axis lengths along the x and y axes, respectively
$\bar{G}_{\text{total}}$	= total strain energy release rate
$\bar{G}_u, \bar{G}_\psi$	= translational and rotational components of strain energy release rate
K^m, K^f	= stress intensity factor at plate midplane and free edge, respectively
K^p, K^u	= stress intensity factor with and without patch, respectively
M_x, M_y	= reaction nodal moments
N_x, N_y, N_z	= reaction nodal forces
r	= debond ellipse aspect ratio b^*/a^*
t_r, t_a, t_s	= thickness of repair, adhesive, and aluminum plate, respectively
u_x^0, u_y^0, u_z^0	= plate midplane displacements in the respective directions
$2a, a$	= total crack length for center and edge crack, respectively
$2L_r$	= overall length of repair
$2L_s$	= overall length of aluminum plate
$2W_r, W_r$	= overall width of repair for center and edge crack, respectively
$2W_s, W_s$	= overall width of aluminum plate for center and edge crack, respectively
Δa	= crack extension length
ψ_x, ψ_y	= rotations of the cross sections perpendicular to the x and y axes

I. Introduction

TO extend the service life of aging aircraft, cracked components must be replaced or repaired. If the number of cracks is small and the crack size is small relative to the size of the component, it is often most economical to employ crack arrestment methods to regain the load carrying capability of the component. A repair method using composite patches to reinforce the cracked structure has been shown to be very promising due to the high stiffness, high strength, and light weight of the composite.[1]

One of the most challenging aspects of bonded composite repair technology is the stress analysis of the repaired structure and the subsequent derivation of stress intensity factors. The difficulty arises from the fact that a plane stress metallic panel under in-plane loading would develop highly complicated three-dimensional stresses if composite patches were bonded to its surfaces either symmetrically (double sided) or unsymmetrically (single sided). The use of three-dimensional finite elements to perform the stress analysis is possible. However, besides the obvious high cost in computation, the need to use elements of high aspect ratios due to the thinness of the adhesive layer and patches can also cause convergence problems. Therefore, most efforts thus far have been directed to developing simplified analysis methods.

For symmetric (double-sided) repairs, many numerical techniques have been used. They include the collocation method,[2,3] boundary element method,[4,5] finite element method,[6,7] finite element alternating method,[8] and approximate analytical solutions.[9] In these methods, the cracked metallic plate is assumed to be in a state of two-dimensional plane stress, and the variation of stresses over the thickness is neglected. The analytical work by Rose would be an efficient solution to the subject problem. However, it has been shown that there are circumstances in which Rose's approximate solutions could yield substantial errors.[10,11] Some methods such as the boundary element method are restricted to isotropic patches.

Unsymmetric repairs present a greater challenge in modeling due to the presence of out-of-plane bending. Ratwani[7] was the first to address the bending effect in an aluminum patch bonded to a cracked aluminum plate. He used two-dimensional plane stress finite elements to solve the single-sided patch problem by neglecting the out-of-plane displacement first. From this result, the loads carried by the cracked plate and patch, respectively, are obtained. The difference of these two loads results in a global moment that is then applied to the entire structure yielding additional stress intensity. Such a correction factor for the bending effect has been suggested for use with Rose's analytic solution.[1] The accuracy of such a correction factor was investigated by Arendt and Sun,[11] who showed appreciable errors could occur, especially if the patch had a much higher modulus than the host structure.

In this study, Mindlin plate finite element is used to model both the host plate and patch. The two plates are connected by adhesive elements. The capability of the plate finite element in modeling bending effects is apparent. Moreover, the inclusion of transverse shear deformation in Mindlin plate theory provides a bilinear displacement approximation through the thickness of the host plate in

Received Feb. 28, 1995; presented as Paper 95-1505 at the AIAA/ASME/ASCE/AHS/ASC 36th Structures, Structural Dynamics, and Materials Conference, New Orleans, LA, April 10–12, 1995; revision received Sept. 15, 1995; accepted for publication Sept. 29, 1995.

*Professor, School of Aeronautics and Astronautics. Fellow AIAA.
†Graduate Student, School of Aeronautics and Astronautics.
‡Student, School of Aeronautics and Astronautics; currently with McDonnell Douglas Aerospace–West, Building 71, MC 71-34, 1510 Hughes Way, Long Beach, CA 90810-1870.

double-sided repair when symmetry is involved in modeling. The efficient crack closure method is used to calculate the strain energy release rate from which the stress intensity factor is derived. A three-dimensional analysis is performed to verify the accuracy of the plate model.

Numerical solutions for single- and double-sided repairs are compared with existing solutions. The double plate model is extended to simulate debonding between the patch and the host plate. Strain energy release rate distribution along the debond front is obtained.

II. Finite Element Model

Figure 1a shows a typical single-sided patch configuration. This can be regarded as the symmetrical half of a double-sided repair. The patch and the plate are modeled as Mindlin plates and the adhesive as linear springs. Figure 1b shows the finite element meshes for the double plate model. The plate nodes are located on the mid-planes of the aluminum plate and patch. The adhesive nodes lie along the patch-adhesive and adhesive-aluminum plate interfaces. The use of effective adhesive properties by Jones and Callinan[6] are no longer necessary, since the spring nodes are separated from the aluminum plate and patch nodes. Constraint equations are imposed on the patch-adhesive and adhesive-aluminum to enforce compatibility along each interface.

The configuration and example finite element mesh for an elliptic debond model are shown in Figs. 2a and 2b, respectively. The mesh shows a quadrant of the composite repair. The same mesh is used for the aluminum plate, except the region between the boundary of the repair mesh and aluminum plate boundary is connected and filled in. A debond crack front is shown in the mesh. Although the composite repair does not contain a crack, the location of the crack in the aluminum plate is shown along the lower boundary.

A. Constraint Equations

The displacement field according to Mindlin plate theory is as follows:

$$\begin{aligned} u_x &= u_x^0 + z\psi_x \\ u_y &= u_y^0 + z\psi_y \\ u_z &= u_z^0 \end{aligned} \tag{1}$$

The adhesive layer is modeled by three linear springs with two nodes located at two interfaces. Each node has three translational degrees of freedom. To ensure displacement continuity along the interfaces, constraint equations are imposed as follows:

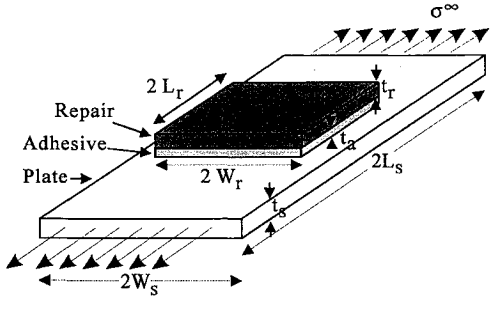

Fig. 1a Sample bonded repair.

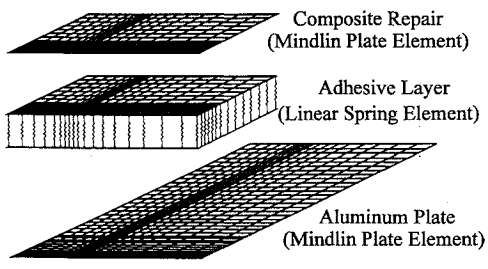

Fig. 1b Finite element model (a quadrant shown).

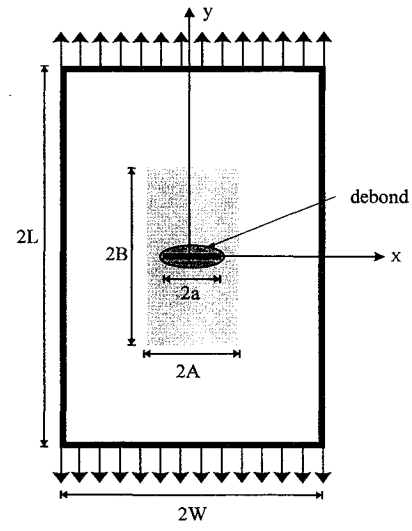

Fig. 2a Configuration of a repaired center crack with debond.

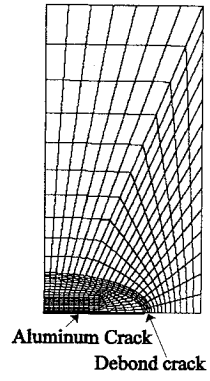

Fig. 2b Finite element mesh with debond (only quadrant of patch region shown).

For the repair-adhesive interface,

$$\begin{aligned} u_x^{01} - (t_r/2)\psi_x^1 &= u_x^{02} \\ u_y^{01} - (t_r/2)\psi_y^1 &= u_y^{02} \\ u_z^{01} &= u_z^{02} \end{aligned} \tag{2a}$$

For the adhesive-plate interface,

$$\begin{aligned} u_x^{03} &= u_x^{04} + (t_s/2)\psi_x^4 \\ u_y^{03} &= u_y^{04} + (t_s/2)\psi_y^4 \\ u_z^{03} &= u_z^{04} \end{aligned} \tag{2b}$$

where superscripts 1 and 4 indicate the kinematic variables in the composite patch and the aluminum plate, respectively; superscripts 2 and 3 indicate the two adhesive spring nodes at the repair-adhesive and adhesive-plate interfaces, respectively. Note that the rotations ψ_x and ψ_y of the repair patch and the aluminum plate are not set equal. Thus, the combined system (patch + plate) does not reduce to a single Mindlin plate.

If there is debond between the patch and the host plate, the constraint equations are removed in the debond region.

B. Adhesive Layer

The adhesive layer is modeled by three springs for the transverse shear stiffness in the x–z and y–z planes and the axial stiffness in the z direction. The shear spring stiffnesses are found from the following approximate shear stresses:

$$\tau_{iz} = \frac{|F_i|}{A} = \frac{G_a|u_i^2 - u_i^3|}{t_a} \tag{3}$$

where τ_{iz} $(i = x, y)$ is the shear stress in the x–z and y–z planes, F_i is the spring force in the x or y directions, A is the area represented by the shear spring, u_i^2 and u_i^3 are the displacements of the upper and lower nodes of the adhesive in the x- and y-directions, and G_a and t_a are the adhesive shear modulus and thickness, respectively. The spring constant, k_i $(i = x, y)$ is obtained as

$$k_i = G_a A / t_a \tag{4}$$

where k_i is the spring stiffness in the x or y direction.

The axial (peel) spring stiffness is derived based on a uniaxial strain assumption, i.e.,

$$\sigma_{zz} = \frac{|F_z|}{A} = \frac{2(1-\nu_a)G_a|u_z^2 - u_z^3|}{(1-2\nu_a)t_a} \tag{5}$$

where F_z is the spring force in the z direction and ν_a is the adhesive Poisson's ratio. From Eq. (5), the axial spring stiffness is obtained as

$$k_z = \frac{2(1-\nu_a)G_a A}{(1-2\nu_a)t_a} \tag{6}$$

Note that the spring constants vary with the element area.

III. Fracture Mechanics

The modified crack closure technique[12] is used to calculate the strain energy release rate. This technique is used for the crack in the aluminum plate and the debond along the adhesive-aluminum interface. It is assumed that the strain energy released during crack extension is equal to the work needed to close the opened crack surfaces. It is also assumed that the adhesive cracks in the aluminum crack region.

In the crack closure method the virtual crack extension Δa is usually taken to be small compared with the crack length. Thus, the nodal displacements (crack opening displacements) at the original crack tip after the extension can be approximated by the nodal displacements at a distance Δa behind the crack tip before the extension. This reduces the analysis to one step instead of two.

In performing the crack closure, the elements in front of and directly behind the crack front should be made similar; i.e., the size of each element both in front of and directly behind the crack front should be equal.

A. Strain Energy Release Rate for Aluminum Crack

The strain energy release rate is computed for mode I fracture loading. The same procedure can be used for mixed mode loading. A four-noded Mindlin plate element is used to model the aluminum plate.

Figure 3 shows a two-dimensional finite element model for the aluminum plate near the crack tip at point b. Assume the crack front extends from b to c. Since the extension Δa is very small, the crack opening displacements at b are taken to be the same as those at a. Thus, the strain energy release rate can be calculated as the work done by the nodal force (moment), F_y^b (M_x^b), in closing the crack opening displacement (rotation), u_y^a (ψ_y^a). The total strain energy release rate is obtained as

$$\bar{G}_{\text{total}} = \bar{G}_u + \bar{G}_\psi \tag{7}$$

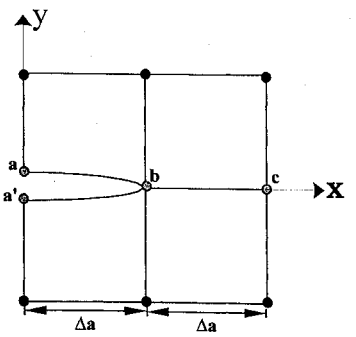

Fig. 3 Aluminum plate crack tip elements (top view).

where

$$\bar{G}_u = (1/2\Delta a)\left\{F_y^b\left(u_y^a - u_y^{a'}\right)\right\}$$

$$\bar{G}_\psi = (1/2\Delta a)\left\{M_x^b\left(\psi_y^a - \psi_y^{a'}\right)\right\}$$

Note that these strain energy release rates are the respective energies released (over the total plate thickness) per crack tip.

B. Stress Intensity Factor

The fracture parameter for the aluminum crack is often given in terms of the stress intensity factor.

If the rotational (bending) contribution to the strain energy release rate $\bar{G}_\psi$ is small, the plane stress relation of the stress intensity factor to the strain energy release rate can be used. We have

$$K_I = K_u = \sqrt{(\bar{G}_u E_s / t_s)} \tag{8}$$

where the subscript s denotes parameters associated with the aluminum plate.

If bending is not negligible, then the plane stress relation given by Eq. (8) may underestimate the maximum value of the stress intensity over the thickness of the plate. Young and Sun[13] used Mindlin plate theory to derive the relation between the mode I total strain energy release rate and the stress intensity factor for pure bending moments. Their result is

$$K_\psi = \sqrt{\frac{3\bar{G}_\psi E_s}{t_s}} \tag{9}$$

where $\bar{G}_\psi$ is the total (rotational) strain energy release rate (per crack tip) and K_ψ is the maximum value of the stress intensity factor (on the tension side of the plate). The maximum stress intensity factor over the thickness of the plate is

$$K_I = K_u + K_\psi \tag{10}$$

Since the stress intensity due to bending is linearly distributed over the thickness of the plate, the stress intensity at any point over the thickness can easily be obtained from the values of K_u and K_ψ.

C. Strain Energy Release Rate for Debond

Cracking along the bond line is a key mode of failure in patch repair. This debond crack may propagate in the adhesive-aluminum or adhesive-patch interface. To predict debond crack growth behavior, the strain energy release rate along the crack front must be evaluated. The present double plate model can be employed to perform this task.

The debond crack always initiates from the location of the original crack in the aluminum plate. Based on some experimental results, we assume that the debond crack lies in the adhesive-aluminum plate interface. In fact, using the present plate model in conjunction with linear springs to represent the adhesive, the strain energy release rates for the two possible debond cracks turn out to be identical. The difference in fracture toughness of these two interfaces would determine the actual location of the debond crack.

To illustrate the procedure for calculating the strain energy release rate, we consider a small region in the neighborhood of the debond crack front. Figure 4 shows part of the finite element model that

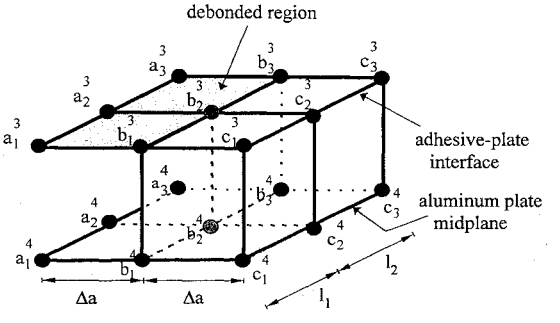

Fig. 4 Schematic of debond crack front.

includes four (four-noded) plate elements for the aluminum plate and nine spring nodes (a_j^3, b_j^3, and c_j^3, $j = 1, 2, 3$). The debond crack front is at the line $b_1 b_2 b_3$. The top (lower adhesive) nodes b_j^3 and c_j^3 are tied to the corresponding bottom (aluminum plate) nodes b_j^4 and c_j^4, respectively, by the constraint conditions in Eq. (2b). The two sets of nodes a_j^3 and a_j^4 are not constrained because of the debond crack. The constraints result in reaction forces N_x, N_y, and N_z and moments M_x and M_y at these nodes. Note that the spring nodes have only reaction forces. The reaction forces and moments at a node are equal to the respective sums of the nodal forces and moments of all of the elements sharing this node.

The closure energy can be determined by assuming that the crack front extends from the current location b_j^3–b_j^4 to c_j^3–c_j^4. Since the extension Δa is very small, the crack opening displacements at b_j^3–b_j^4 are taken to be the same as those at a_j^3 and a_j^4 before the assumed crack extension. Thus, the crack closure energy associated with a pair of nodes (say b_2^3 and b_2^4) can be expressed in the form

$$2U_{b_2} = N_x^3 \Delta u_x^3 + N_y^3 \Delta u_y^3 + N_x^3 \Delta u_x^3 + N_x^4 \Delta u_x^4 + N_y^4 \Delta u_y^4 + N_z^4 \Delta u_z^4 + M_x^4 \Delta \psi_x^4 + M_y^4 \Delta \psi_y^4 \tag{11}$$

where N_i^3 and N_i^4 (M_i^4) are nodal constraining forces (moments) before crack extension at nodes b_2^3 and b_2^4, respectively, and u_i^3 and u_i^4 (ψ_i^4) are the nodal displacements (rotations) at nodes a_j^3 and a_j^4, respectively. Also, Δu_i^3 denotes the difference of the nodal displacements between nodes a_j^3 and b_j^3, and Δu_i^4 denotes the relative displacements between nodes a_j^4 and b_j^4.

The strain energy released over an area associated with the assumed crack extension can be calculated using Eq. (11). The average strain energy release rate is obtained by dividing the total strain energy released by the local area. For example, the total strain energy release rate at b_2 is calculated as

$$G = \left(U_{b_2}/A\right) \tag{12}$$

where

$$A = \Delta a \times \frac{(l_1 + l_2)}{2}$$

The accuracy of such calculation depends on the finite element mesh, especially at the crack front. A similar procedure as just described was used by Klug et al.[14] to calculate the strain energy release rate at the delamination front in laminated composites with excellent accuracy.

IV. Results

A. Symmetric Repair

The commercial finite element code ABAQUS is used to perform the analysis using the double plate model. The first comparison is with a double-sided repair of an edge crack in a rectangular plate subjected to a uniform tensile load. The cracked plate is repaired with an aluminum patch. This problem has been investigated by Young et al.[5] using the boundary element method in which the cracked aluminum plate was assumed to be in a state of plane stress. In the present analysis, the model is established for half of the entire configuration that is divided by the midplane of the aluminum plate. Thus, the aluminum plate is actually modeled by two Mindlin plates allowing bilinear displacements through the thickness.

The material properties and dimensions (see right half of the plate in Fig. 2a) are as follows: aluminum plate: $E_s = 70.0$ GPa and $\nu_s = 0.3$, dimensions: $L_s = W_s = 90$ mm and $t_s = 1.5$ mm, patch: $E_r = 70$ GPa and $\nu_r = 0.3$, dimensions: $L_r = W_r = 30$ mm and $t_r = 1.5$ mm, and adhesive: $G_a = 0.6$ GPa, $\nu_a = 0.3$, and $t_a = 0.15$ mm.

The unpatched configuration is analyzed first. Table 1 shows the normalized stress intensity denoted by K^u. The stress intensity factor is normalized as follows:

$$K = K_I/(\sigma\sqrt{\pi a}) \tag{13}$$

where σ is the uniform applied tensile load and a is the crack length.

Table 1 Comparison of K^u for unpatched edge crack

	K^u		
a, mm	Exact	Young[5]	Present
14.99	1.297	1.297	1.297
29.99	1.786	1.791	1.788

Table 2 Comparision of K^p for patched edge crack

	K^p	
a, mm	Young[5]	Present
14.99	0.207	0.208
29.99	0.188	0.190

Table 3 Comparison of K for double-sided patch

	K		
λ	Chue[15]	Present plate	Present three-dimensional solutions
−2	0.196	0.223	0.239
0	0.215	0.246	0.263
2	0.234	0.269	0.287

Table 2 shows the normalized stress intensity factors for the patched configurations indicated by K^p.

The numerical results from the double plate model indicate that the contribution of bending (rotation) to the strain energy release rate is very small and can be neglected. The results also indicate that the in-plane displacements in the aluminum plate including the crack surfaces are quite uniform over the thickness. Thus, the plane stress assumption for double-sided repairs is valid.

B. Comparison to Three-Dimensional Solution

Recently, Chue et al.[15] presented numerical results for single-sided and double-sided repairs under biaxial loading using 20-noded isoparametric three-dimensional brick elements. To avoid numerical ill-conditioning possibly resulting from the use of elements (for the adhesive) with high aspect ratios, a reduced integration technique was invoked. The stress singularity at the crack tip was induced by shifting the side nodes to the quarter-point position. The crack was assumed to be located at the center of the plate with an inclined orientation. In the present study, only the horizontal crack (parallel to the x axis) is considered.

To provide additional comparisons, we also perform an independent three-dimensional finite element analysis using ABAQUS. The strain energy release rate using a 20-noded brick element is computed with the same technique used by Whitcomb.[16] The through-the-thickness distribution of the strain energy release rate is computed at the corner nodes of each element. The strain energy release rate is converted into the stress intensity factor by assuming that the local stress field near the crack front is in a state of plane strain. Consequently, the relation between strain energy release rate and stress intensity factor is

$$K_I = \sqrt{\frac{G}{E(1-\nu^2)}} \tag{14}$$

Thus, the distribution of the stress intensity factor through-the-thickness of the plate can be obtained.

The material properties and plate dimensions considered here are identical to those used by Chue.[15] They are listed as follows: aluminum plate: $E_s = 71.02$ GPa and $\nu_s = 0.32$; dimensions: $L_s = 180$ mm, $W_s = 120$ mm, $t_s = 2.29$ mm; boron composite patch: $E_1 = 208$ GPa, $E_2 = E_3 = 25.44$ GPa, $G_{12} = G_{13} = 7.24$ GPa, $G_{23} = 4.94$ GPa, $\nu_{12} = \nu_{13} = 0.1677$, and $\nu_{23} = 0.0350$; dimensions: $L_r = 76$ mm, $W_r = 38$ mm, and $t_r = 0.127$ mm (double sided) and 0.762 mm (single sided); adhesive: $G_a = 0.965$ GPa, $\nu_a = 0.32$, and $t_a = 0.1016$ mm; and crack length: $a = 25$ mm.

The comparison for the double-sided repair is shown in Table 3. The biaxial load factor λ is defined as the ratio of the uniform tensile

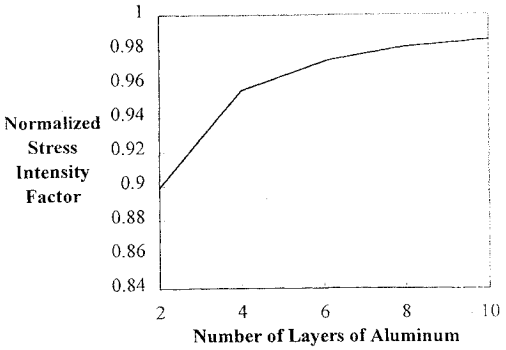

Fig. 5 Convergence of number of layers of three-dimensional elements through-the-thickness of aluminum plate ($\lambda = 0$) for single-sided repair.

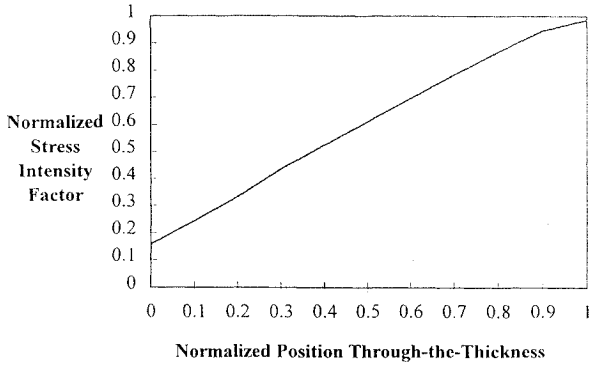

Fig. 6 Distribution of normalized stress intensity factor through-the-thickness of aluminum plate ($\lambda = 0$) for single-sided repair.

loading in the x direction to that in the y direction. The normalized stress intensity factor is defined as

$$K = \frac{K_I}{\sigma_y \sqrt{\pi a}} \tag{15}$$

where σ_y is the loading stress in the y direction. Note that this stress intensity factor is taken at the midplane of the aluminum plate. The present three-dimensional solutions for K are significantly larger than those obtained by Chue et al.[15] The plate model yields solutions in good agreement with the present three-dimensional solutions.

A convergence study for a single-sided patch shown in Fig. 5 illustrates the normalized stress intensity factor at the aluminum plate free edge vs the number of three-dimensional elements through-the-thickness of the aluminum plate. The result indicates that about 10 elements are required to obtain accurate results for the stress intensity factor in bending. However, we should note that the accuracy of the technique used to compute the stress intensity factor also depends on the planar mesh at the crack front. Note that the value of the strain energy release rate at each corner is locally averaged. Half of the work done at each of the two adjacent midside nodes is added to the work at the corner node. The final distribution of the normalized stress intensity factor through-the-thickness is shown in Fig. 6. The zero position is at the adhesive-aluminum interface. It is evident that the distribution of the stress intensity factor through the plate thickness is nearly linear. This result supports the use of plate elements that assume a linear distribution of bending stress over the plate thickness.

Comparisons of the single-sided repair stress intensity factor are made at the plate midplane and free edge. Table 4 lists the normalized stress intensity factor at the midplane K^m, and Table 5 lists the normalized stress intensity factor at the free surface of the plate K^f. Appreciable differences between the two values are noted indicating a strong bending effect.

Comparing the three solutions, it is interesting to note that the plate model solution always lies between the two three-dimensional finite element solutions that differ substantially. The plate solution, however, agrees better with our own three-dimensional solution, especially for the stress intensity factor at the free surface of the plate. The difference between the plate solution and the present three-dimensional solution could be due to the difference in the adhesive modeling.

On the other hand, no convergence study was mentioned by Chue et al. It is difficult to assess the accuracy of their three-dimensional finite element solutions. Judging from a typical finite element mesh shown in their paper, it appears that only two elements over the plate thickness were used. With such a coarse mesh, the low values of the stress intensity factor are quite possible, especially if the bending effect is significant, such as in the single-sided repair.

Table 4 Comparison of K^m at the midplane for single-sided repair

	K^m		
λ	Chue[15]	Present plate	Present three-dimensional solutions
−2	0.392	0.493	0.565
0	0.481	0.536	0.612
2	0.571	0.579	0.660

Table 5 Comparison of K^f at the free surface for single-sided repair

	K^f		
λ	Chue[15]	Present plate	Present three-dimensional solutions
−2	0.742	0.900	0.933
0	0.902	0.953	0.985
2	1.062	1.007	1.036

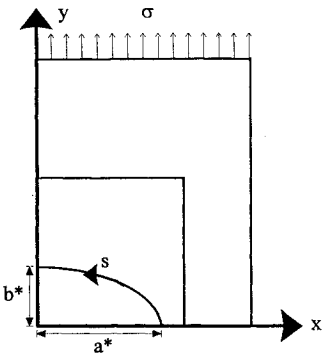

Fig. 7 Quadrant of debond crack front configuration.

C. Debond Crack

The debond crack front is modeled as an ellipse. The material properties and geometry from Sec. IV.B, except for crack length and patch thickness, are used for the analysis. The patch thicknesses for the double- and single-sided repairs are 0.127 and 0.254 mm, respectively. The debond is assumed to lie along the aluminum-adhesive interface. The distribution of the strain energy release rate is computed according to Sec. III.C.

Figure 7 illustrates the geometry of a quarter of the patched plate. The normalized arc length of the debond is defined with the zero point at the x axis. The semimajor axis of the debond a^* is 25 mm. Two values of the semiminor axis b^* are chosen as 8.75 mm and 10.0 mm. The debond aspect ratio r is defined as $r = a^*/b^*$. The aluminum crack length a is 4% shorter than a^*, and its tip is behind the debond crack. The applied stress is $\sigma = 0.689$ MPa.

Figures 8 and 9 show the distributions of the strain energy release rate for double-sided and single-sided repairs, respectively. It is interesting to note that, for the same loading and amount of patching material, the debond strain energy release rate in the double-sided repair is greater than that in the single-sided repair. This indicates, to our surprise, that the debond crack is more likely to grow in the double-sided repair if the total strain energy release (without considering mode mixity) governs crack growth.

From Fig. 8 it is seen that near the aluminum crack tip the strain energy release rate at the debond crack front approaches zero. This indicates that a debond crack is unlikely ahead of the aluminum crack. However, this is not true for the single-sided repair as shown by the result in Fig. 9.

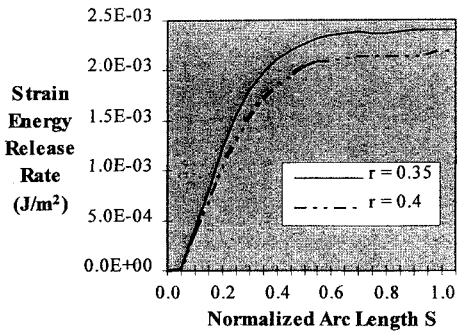

Fig. 8 Debond crack strain energy release rate distributions for double-sided patch.

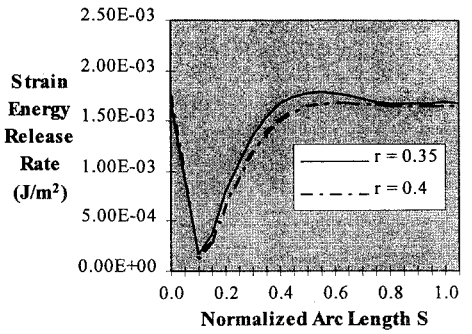

Fig. 9 Debond crack strain energy release rate distributions for single-sided patch.

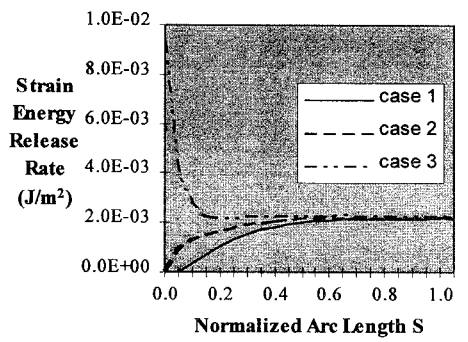

Fig. 10 Distribution of debond crack strain energy release rate for double-sided patch with varying locations of aluminum crack tip.

To further investigate the effect of the relative position between the debond crack front and the aluminum crack tip location, we consider the double-sided repair. The following cases are considered: case 1, $a = (1 - 0.04)a^*$; case 2, $a = a^*$; and case 3, $a = (1 + 0.04)a^*$. For all cases, $r = b^*/a^* = 0.4$ is used. The result presented in Fig. 10 indicates that it is unlikely that the debond crack front would grow far ahead of the aluminum crack tip.

The exact shape of the debond crack is one that yields a constant strain energy release rate distribution along the crack front. From Figs. 8 and 10, it can be concluded that the debond crack is approximately elliptical except for the region near the aluminum crack tip. Elliptical debonds have been experimentally observed by Ratwani.[7] Also, Poole et al.[17] and Baker[18] observed elliptic debonds in double-sided repairs and noted that the aluminum crack tip and debond crack were in the same vicinity.

V. Conclusions

A finite element based double-plate model has been presented for analysis of strain energy release rates in cracked plates with bonded patches. In calculating the stress intensity factor in plates with double-sided patches, the present model showed excellent agreement with existing boundary element solutions and three-dimensional finite element solutions. For plates with a single-sided patch, there are appreciable discrepancies between the stress intensity factors obtained using the present plate model and a three-dimensional finite element model. These discrepancies could result from the different models used to represent the adhesive layer.

In this study it has also been demonstrated that the double-plate model can be used to analyze a debond crack between the adhesive and the plate or the patch. Given a debond crack, the strain energy release rate along the crack front can be calculated. This numerical capability allows one to determine the size of debond region for a given static load and interface fracture toughness or to determine debond crack growth under fatigue loading.

Acknowledgment

This work was supported by the U.S. Air Force Office of Scientific Research through University Research Initiative Grant F49620-93-0377 to Purdue University.

References

[1]Baker, A. A., and Jones, R., *Bonded Repair of Aircraft Structure*, Martinus–Nijhoff Publishers, Dordrecht, The Netherlands, 1988.

[2]Dowrick, G., Cartwright, D. J., and Rooke, D. P., "The Effects of Repair Patches on the Stress Distribution in a Cracked Sheet," *Proceedings of the 2nd International Conference on Numerical Methods in Fracture Mechanics* (Swansea, Wales, UK), edited by D. R. J. Owen and A. R. Luxmore, 1980, pp. 763–775.

[3]Young, A., Cartwright, D. J., and Rooke, D. P., "Model Studies of Repair Patches," *Proceedings of the ASM International Conference on Fatigue, Corrosion Cracking, Fracture Mechanics, Fracture Mechanics and Failure Analysis* (Salt Lake City, UT), Vol. 92, Metals Park, OH, 1986, pp. 339–346.

[4]Young, A., Cartwright, D. J., and Rooke, D. P., "The Boundary Element Method for Analyzing Repair Patches on Cracked Finite Sheets," *Aeronautical Journal of the Royal Aeronautical Society*, Dec. 1988, pp. 416–421.

[5]Young, A., Rooke, D. P., and Cartwright, D. J., "Analysis of Patched and Stiffened Cracked Panels Using the Boundary Element Method," *International Journal of Solid Structures*, Vol. 29, No. 17, 1992, pp. 2201–2216.

[6]Jones, R., and Callinan, R. J., "A Design Study in Crack Patching," *Fiber Science and Technology*, Vol. 14, 1981, pp. 99–111.

[7]Ratwani, M. M., "Characterization of Fatigue Crack Growth in Bonded Structures," Air Force Flight Dynamics Lab., AFFDL-TR-77-31, Vols. 1 and 2, Wright–Patterson AFB, OH, June 1977.

[8]Park, J. H., Ogiso, T., and Atluri, S. N., "Analysis of Cracks in Aging Aircraft Structures, with and without Composite-Patch Repairs," *Computational Mechanics*, Vol. 10, Nos. 3, 4, 1992, pp. 169–201.

[9]Rose, L. R. F., "An Application of the Inclusion Analysis for Bonded Reinforcements," *International Journal of Solids and Structures*, Vol. 17, No. 8, 1981, pp. 827–838.

[10]Young, A., Rooke, D. P., and Cartwright, D. J., "Numerical Study of Balanced Patch Repairs to Cracked Sheets," *Aeronautical Journal of the Royal Aeronautical Society*, Vol. 93, Nov. 1989, pp. 327–333.

[11]Arendt, C., and Sun, C. T., "Bending Effects of Unsymmetric Adhesively Bonded Composite Repairs on Cracked Aluminum Panels," *Proceedings of the FAA/NASA International Symposium on Advanced Structural Integrity Methods for Airframe Durability and Damage Tolerance* (Hampton, VA), Pt. 1, 1994, pp. 33–48.

[12]Rybicki, E. F., and Kanninen, M. F., "A Finite Element Calculation of Stress Intensity Factors by a Modified Crack Closure Integral," *Engineering Fracture Mechanics*, Vol. 9, No. 9, 1977, pp. 931–938.

[13]Young, M. J., and Sun, C. T., "On the Strain Energy Release Rate for a Cracked Plate Subjected to Out-of-Plane Bending Moment," *International Journal of Fracture*, Vol. 60, No. 3, 1993, pp. 227–247.

[14]Klug, J., Wu, X. X., and Sun, C. T., "Efficient Modeling of Delamination Growth in Composite Laminates Using Plate Elements," *Symposium on the Durability of Composite Materials*, edited by R. C. Wetherhold, ASME publication MD-Vol. 51, American Society of Mechanical Engineers, New York, 1994, pp. 177–189.

[15]Chue, C. H., Chang, L. C., and Tsai, J. S., "Bonded Repair of a Plate with Inclined Central Crack Under Biaxial Loading," *Composite Structures*, Vol. 28, No. 1, 1994, pp. 39–45.

[16]Whitcomb, J. D., "Three-Dimensional Analysis of a Postbuckled Embedded Delamination," *Journal of Composite Materials*, Vol. 23, No. 9, 1989, pp. 862–889.

[17]Poole, P., Lock, D., and Young, A., "Composite Patch Repair of Thick Aluminum Alloy Sections," *International Conference on Aircraft Damage Assessment and Repair* (Melbourne, Australia), 1991, pp. 85–91.

[18]Baker, A. A., "Fatigue Crack Propagation Studies on Aluminum Panels Patched with Boron/Epoxy Composites," *International Conference on Aircraft Damage Assessment and Repair* (Melbourne, Australia), edited by R. Jones and N. J. Miller, Inst. of Engineers, 1991, pp. 209–215.